

Surface $p\text{CO}_2$ and hydrography in the dense water formation area of the southern Adriatic

Carlotta Dentico^{1,2}, Angelo Rubino¹, Giuseppe Civitarese², Michele Giani², Giuseppe Siena², Stefano Kuchler², Julien Le Meur², Andrea Corbo² and Vanessa Cardin²

¹ Department of Environmental Sciences, Informatics and Statistics, Università Cà Foscari, Venice, Italy

² National Institute of Oceanography and Applied Geophysics (OGS), Trieste, Italy

Correspondence to: Carlotta Dentico (cdentico@ogs.it)

Abstract.

The rising CO_2 concentration in the atmosphere leads to an increase in CO_2 uptake by the ocean and to significant changes in seawater chemistry. These changes, in turn, exert profound effects on marine ecosystems across multiple trophic levels. The Mediterranean Sea is considered a hotspot for climate change. Despite such relevance, observations and studies on its carbonate system remain limited, especially in regions that play a crucial role in regulating air-sea CO_2 exchange such as intermediate and dense water formation areas. The southern Adriatic Sea, a key site for dense water formation in the eastern Mediterranean, hosts the EMSO ERIC and ICOS ERIC South Adriatic observatory (EMSO-E2M3A), operated by the Italian National Institute of Oceanography and Applied Geophysics (OGS). This facility allows the study of physical and biogeochemical dynamics in the deepest area of the Adriatic Sea. The suite of sensors deployed on the surface buoy allows for the characterization of water mass properties, biogeochemical cycles, dense water formation process, and ocean acidification, particularly in relation to carbon sequestration dynamics. Here, time series of meteorological data (e.g., wind speed, wind direction), sea surface physical parameters (e.g., temperature, salinity), dissolved oxygen and partial pressure of CO_2 ($p\text{CO}_{2\text{sw}}$) and pH from 2014 to 2024 will be presented (<https://doi.org/10.13120/y2hw-1j63>, Cardin et al., 2025b). In particular, quality check, correction and post-processing methods applied to the data will be discussed. The validated surface dataset provides a consistent $p\text{CO}_{2\text{sw}}$ time series for the Adriatic Sea, with values and seasonal variability in agreement with previous observations across the Mediterranean. Associated temperature, salinity, oxygen, and wind measurements reproduce expected regional patterns, confirming the robustness and suitability of the presented dataset for further biogeochemical and climate-related analyses.

1. Introduction

The concentration of CO_2 in the atmosphere has rapidly increased from around 280 parts per million (ppm) at the beginning of the Industrial Revolution in 1750, to 427 ppm in February 2025 (<http://co2.earth/>). This increase is the primary driver of the intensification of the ocean CO_2 sink, which has increased from $1.2 \pm 0.4 \text{ GtC yr}^{-1}$ in the 1960s to $2.9 \pm 0.4 \text{ GtC yr}^{-1}$ in the period 2014 - 2023 (Friedlingstein et al., 2025). However, the net air-sea CO_2 flux is a highly dynamic process exhibiting significant spatial and temporal heterogeneity driven by complex natural and anthropogenic processes (Takahashi et al., 2009; Friedlingstein et al., 2025).

38 This accelerated oceanic CO₂ uptake is the direct cause of changes in seawater chemistry commonly referred to
39 as ocean acidification (OA). These changes are associated with a reduction in seawater pH and carbonate ion
40 concentrations, and an increase in dissolved CO₂, dissolved inorganic carbon and bicarbonate ions (Orr et al.,
41 2015). OA poses a significant threat to marine ecological communities (e.g., Gattuso and Hansson, 2011; Riebesell
42 et al., 2013; IPCC, 2021), which rely on specific ranges of key carbonate chemistry parameters for their survival.
43 Continuous, high-quality ocean carbon data are therefore essential to monitor these changes, predict future
44 impacts, and contribute to the biogeochemical Essential Ocean Variables (EOVs) framework of the Global Ocean
45 Observing System (GOOS).

46 The Mediterranean Sea is a recognized climate change hotspot (e.g., Zittis et al., 2019; Urdiales-Flores et al.,
47 2023; Lazoglou et al., 2024). The unique hydrological and biogeochemical characteristics of the Mediterranean
48 Sea waters (Alvarez et al., 2023) enhance the uptake and transfer of CO₂ to depth more efficiently than the global
49 ocean (Schneider et al., 2010; Hassoun et al., 2015), with anthropogenic CO₂ having already penetrated all major
50 water masses of the basin (Touratier and Goyet, 2011; Hassoun et al., 2015; Ingrosso et al., 2017). Research has
51 shown that the Mediterranean Sea is already experiencing negative pH trends (e.g., Hassoun et al., 2015;
52 Kapsenberg et al., 2017; Cantoni et al., 2024; Garcia-Ibanez et al., 2024), often with a wider range than those
53 observed in the Atlantic Ocean. However, reliable biochemical and biological carbonate system data remain
54 limited (Hassoun et al. 2022), and comprehensive OA data are still sparse, not easily accessible and often not
55 scalable. Within the Mediterranean, the southern Adriatic Sea is a particularly critical region, serving as the
56 primary site for dense water formation in the eastern Mediterranean (Robinson et al., 2001). About 82% of the
57 Adriatic Dense Water (AdDW) is formed by winter convection (Ingrosso et al., 2017), while the remaining part
58 has its origin on the northern Adriatic shelf and in the middle Adriatic (Ovchinnikov et al., 1985; Bignami et al.,
59 1990; Malanotte-Rizzoli, 1991). The Northern Adriatic Dense Water (NAdDW) is formed in winter, due to the
60 cooling of the entire water column caused by E-NE wind (named Bora). Winter convection and intense Bora
61 winds produce the densest (potential density anomaly, $\sigma_\theta = 29.2 \text{ kg m}^{-3}$) water mass in the Mediterranean Sea
62 (Malanotte-Rizzoli, 1991; Artegiani et al., 1997). These meteorological and oceanographic conditions which
63 favour heat loss, can also favour CO₂ dissolution when surface water is undersaturated with respect to the
64 overlying atmosphere (Cantoni et al., 2024). The NAdDW is partially collected in the middle Adriatic and partly
65 flows southward to the deepest part of the southern Adriatic, ventilating the deep southern Adriatic Pit (Cardin et
66 al., 2011; Cantoni et al., 2016; Le Meur et al., 2025). Previous studies have demonstrated that NAdDW enriched
67 in CO₂ water mass cascades in the southern Adriatic deepest layers and mixes with ambient waters, leading to
68 substantial modifications of the CO₂ content of AdDW (Cantoni et al., 2016; Ingrosso et al., 2017). Additionally,
69 Ingrosso et al. (2017) provided the first observational evidence of the role of southern Adriatic dense water
70 formation in the sequestration of anthropogenic CO₂, capturing conditions indicative of vertical convection and
71 CO₂ accumulation at intermediate depths. These findings highlight the importance of sustained observations for
72 understanding carbon dynamics in this dense water formation region. In this context, the physical and
73 biogeochemical properties of the southern Adriatic Sea (SAd) are monitored through coordinated open-ocean
74 observations, including research vessels, moorings, and autonomous platforms such as ocean gliders and Argo
75 floats. Here, meteorological, physical and biogeochemical data collected by the EMSO ERIC and ICOS ERIC
76 South Adriatic observatory named EMSO-E2M3A, operated by the Italian National Institute of Oceanography
77 and Applied Geophysics (OGS) will be presented. EMSO-E2M3A is part of the European Multidisciplinary

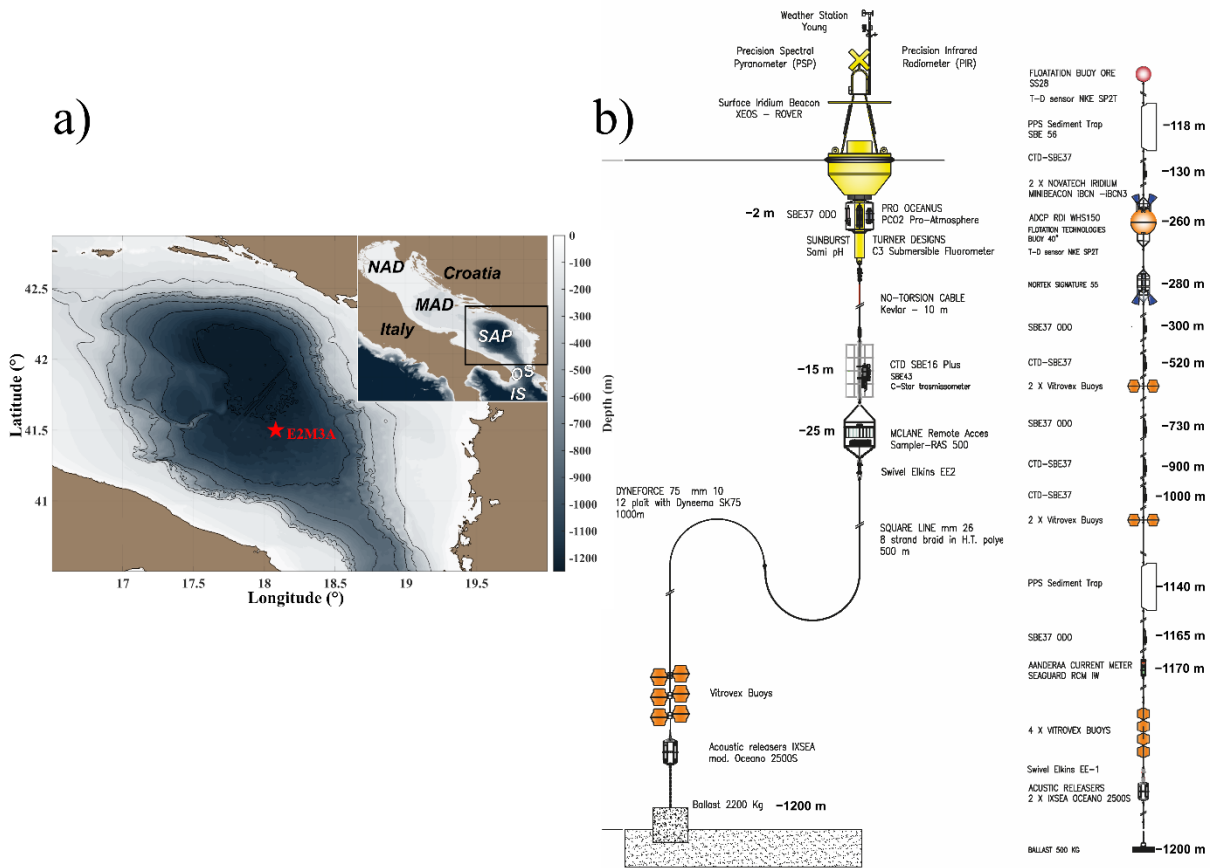
78 Seafloor and Water Column (EMSO) - South Adriatic Regional Facility - (EMSO ERIC) and of the Integrated
79 Carbon Observation System (ICOS) networks. It has been in operation since 2006 representing the longest open-
80 ocean time series in the whole Adriatic making it an ideal site for the investigations of several physical (Bensi et
81 al., 2013, 2014; Cardin et al., 2020; Amorim et al., 2024; Le Meur et al., 2025) and biogeochemical processes
82 (Ingrosso et al., 2017) in the whole water column, as well as air-sea interactions. The time series presented here
83 represents an important resource to understand physical and biogeochemical changes occurring in the region, the
84 OA and the biological responses of planktonic organisms, and to evaluate biogeochemical model performance. A
85 potential use of this time series will also be discussed, in particular related to the calculation of sea-air CO₂ flux
86 and the associated uncertainties. Ultimately, this dataset and its potential applications will contribute to assess the
87 role of the southern Adriatic in regulating CO₂ exchange and to quantify the carbon stored in the deep layers.

88 2. Material and methods

89 2.1. Study area

90 The southern Adriatic (SAd) is the deepest part of the Adriatic Sea, with the southern Adriatic Pit (SAP) reaching
91 maximum depths of approximately 1250 m (Figure 1a). This area is featured by a quasi-permanent cyclonic
92 circulation, and dense water formation takes place at the centre of the gyre through winter open-ocean convection
93 (Ovchinnikov et al., 1985; Gačić et al., 1997) contributing to the eastern Mediterranean thermohaline circulation
94 (Robinson et al., 2001). Different water masses can be distinguished in the SAd: i) the Adriatic Surface Water
95 (AdSW) is a relatively fresh and warm water mass, which originates from the Po River runoff and flows southward
96 along a narrow coastal layer of the western Italian shelf and exits through the Strait of Otranto; ii) the Ionian
97 Surface Water (ISW), entering the basin in the eastern part of the Otranto Strait, can be found in the upper part of
98 the water column; iii) Eastern Intermediate Water (EIW) which is not a water mass per se, but the combination of
99 Levantine Intermediate Water (LIW) and Cretan Intermediate Water (CIW; Schroeder et al., 2024); iv) the
100 Adriatic Deep Water (AdDW), which represents one of the main components of deep waters for the whole Eastern
101 Mediterranean basin (Schlitzer et al., 1991; Roether and Schlitzer, 1991; Schroeder et al., 2024), and occupies the
102 bottom layer of the SAP. The hydrological and biogeochemical dynamics of the SAd are strictly linked to that of
103 the Ionian Sea (IS) by means of the Bimodal Oscillating System (BiOS) that changes the circulation of the North
104 Ionian Gyre (NIG) from cyclonic to anticyclonic and vice versa, on decadal time scale (Gačić et al., 2011;
105 Civitarese et al., 2023). The anticyclonic phase of the NIG leads to the entrance of the Atlantic Water, which
106 decreases the salinity and the density of the AdDW. The cyclonic phase brings warm and salty EIW and Levantine
107 Surface Water in the basin increasing the salinity (and density) of the outflowing AdDW into the IS that gradually
108 impairs the cyclonic NIG, eventually reversing it to an anticyclone.

109 The physical and biogeochemical data presented here were measured by surface sensors deployed at the EMSO-
110 E2M3A regional facility. The site is located in the center of the SAP (nominal position 41.5053°N, 18.0806°E;
111 Figure 1a) and it is composed of two independent mooring lines (Figure 1b). The primary mooring line hosts a
112 surface buoy allowing real-time transmission of meteorological, and ocean surface hydrological and
113 biogeochemical data. The secondary mooring is composed of an array of sensors positioned at several depths
114 aimed at measuring physical and biogeochemical parameters, from the seafloor to the upper layer (Cardin et al.,
115 2025a). Further information on the site can be found in Bozzano et al. (2013) and Ravaioli et al. (2016).



117

118

119 **Figure 1.** a) Map of the study area with the location of EMSO-E2M3A station (nominal position 41.5053°N, 18.0806°E)
 120 represented by the red star moored in the South Adriatic Pit. Geographical indications of the Southern Adriatic Pit (SAP), the
 121 Otranto Strait (OS), Ionian Sea (IS), Middle Adriatic (MAD) and northern Adriatic (NAD) are provided. b) Scheme of the
 122 surface buoy and of the deep mooring with the depths of the different instruments.

123 **2.2. Data collection and quality check**

124 Time series from autonomous sensors at key locations are fundamental components of the GOOS
 125 (<https://www.ioc.unesco.org/>). They provide a continuous view of the temporal behaviour of the system on long-
 126 term baselines, enabling the measurement of a wide range of interrelated variables, promoting the sharing of data,
 127 as demonstrated by international initiatives such as MonGOOS (The Mediterranean Oceanographic Network for
 128 the Global Ocean Observing System), OceanSITES and FixO3 (Fixed point Open Ocean Observatory network,
 129 FP7 EUProject). Nevertheless, the data, acquired by sensors on ocean observing infrastructures, require quality
 130 controls according to defined standards to serve as reliable reference points. In the next sections, a detailed
 131 description of the data quality procedures applied to the data will be discussed.

132 **2.2.1. Meteorological data**

133 Meteorological high-frequency (hourly) data were collected by Young (R.M. Young Company) sensors on the
 134 meteorological station located on the surface buoy. These data include: air temperature (°C), wind speed (m/s),
 135 wind gust (m/s), wind direction (°deg), air pressure (hPa), relative humidity (%) and long and short wave radiation

136 (W/m²). Horizontal wind speed and direction have been measured by a Wind Monitor-MA (model 05106), with
137 manufacturer stated accuracy of ± 0.3 m/s and ± 3 degrees respectively, pressure is measured by a barometric
138 pressure sensor (model 61402V) with manufacturer stated digital accuracy of 0.2 hPa (at 25°C) and 0.3 hPa (-
139 40°C to +60°C) and analog accuracy of 0.05% of analog pressure range, and relative humidity and air temperature
140 were measured by a Relative Humidity/Temperature Probe (model 41382VC) with manufacturer stated accuracy
141 equals to $\pm 0.1\%$ (at 23°C) and $\pm 0.3^\circ\text{C}$ (at 23°C) respectively. Data have been corrected and quality controlled
142 following the procedure described in Cardin et al. (2014). This procedure consists of a series of tests on the data
143 to identify erroneous and anomalous values to establish if the data have been corrupted. Checks on individual or
144 consecutive data points provide information for instrument errors, and checks on regional ranges, consistency
145 with physical limits of the data (spikes), rate of change, and stationarity of data were also performed. No editing
146 of invalid data and replacement of missing data are performed, but only a flag is given to the data at each of the
147 automatic quality control checks.

148 **2.2.2. CTD data**

149 Temperature (°C), salinity (Sal) and dissolved oxygen (DO, $\mu\text{mol/kg}$) high-frequency data (hourly) were collected
150 by a CTD (Conductivity-Temperature-Depth) SeaBird SBE 37-ODO probe at 2 m depth. The SBE 37-ODO is a
151 high-accuracy conductivity and temperature recorder that includes an Optical Dissolved Oxygen (DO) sensor
152 (SBE63). The instrument has a manufacturer stated accuracy of $\pm 0.002^\circ\text{C}$, ± 0.003 mS/cm and $\pm 0.1\%$ of full
153 scale, for temperature, conductivity and oxygen respectively. The data underwent an initial quality control as
154 described in Cardin et al. (2014). First, a physical range test is applied to the data to control the physical
155 significance of each parameter. Given the general increase in salinity in the SAP, as reported by Amorim et al.
156 (2024) and Le Meur et al. (2025), a modified salinity threshold than Cardin et al., (2014) was applied (39.5 instead
157 of 39). Despiking was then performed to highlight the values having a difference with neighbouring values greater
158 than the defined threshold. Finally, a rate of change test was performed as the final step of the initial quality control
159 procedure. While despiking identifies isolated outliers that differ significantly from the neighbouring values, the
160 rate of change identifies fluctuations that are too rapid. After this step, linear interpolation was applied to data
161 gaps greater than 6 hours. While the first quality control consisted of statistical analyses, the second quality control
162 procedure focused on the comparison between SBE 37-ODO time series and reference data collected during
163 oceanographic cruises. For temperature and conductivity (salinity), fourteen corrected CTD casts performed near
164 EMSO-E2M3A from 02/11/2015 to 31/10/2024 were used. The CTD casts were corrected according to the post-
165 processing methods suggested by the manufacturer (SeaBird software). These CTD casts were taken as reference
166 as they have a higher accuracy and higher vertical resolution than the data measured by the SBE 37-ODO. The
167 time series were compared with the reference CTD casts to detect any offset, which, if present, was added to the
168 time series. Another type of error that can affect a time series and needs to be corrected is the drift of the
169 instrument. Particular attention should be paid to the natural variability and trend of the different variables
170 characterizing the dynamics occurring in the area. In this case, the drift was calculated considering both short time
171 periods, and the entire time span of the SBE 37-ODO time series. Calculating the drift only over a short time
172 scale, that may result from an episodic physical process, is not representative of the long-term natural trend. DO
173 ($\mu\text{mol/kg}$) data were quality checked by comparing the probe data with DO ($\mu\text{mol/kg}$) from discrete samples
174 collected at the EMSO-E2M3A station. Samples for the determination of DO were collected in calibrated 50 ml

175 bottles and DO was determined by the Winkler potentiometric titration method (Oudot et al., 1988). The precision
 176 of the measurements was evaluated on three to five replicates collected from the same Niskin bottle, and was, on
 177 average, 0.08%. Before the comparison with reference seawater samples, post-processing of DO data follows the
 178 same quality control procedures applied to temperature and conductivity (salinity). However, an additional quality
 179 control step for DO was introduced before the second quality control to account for the adjustment time of the
 180 oxygen sensor at switch-on. It consisted of fitting a double exponential function and flagging initial values that
 181 deviated significantly from the long-term behavior. The comparison was possible with a limited number of
 182 samples, which revealed a mean difference between DO from discrete samples and DO measured by the probe of
 183 $-9.36 \mu\text{mol/kg}$ (-0.21 mL/L) with a maximum difference of $-10.35 \mu\text{mol/kg}$ (-0.232 mL/L). Further information
 184 on the correction methods applied can be found in Bensi et al., (2012, 2014), Cardin et al. (2020), Amorim et al.,
 185 (2024) and Le Meur et al., (2025).

186 2.2.3. Sea surface $p\text{CO}_2$

187 Since 2014, a Pro-Oceanus CO_2 -Pro sensor has provided high-frequency (every 4 hours) autonomous
 188 measurements of $p\text{CO}_2$ in water ($p\text{CO}_{2\text{sw}}$, μatm) at a depth of approximately 2 meters. In 2023, a Pro-Oceanus
 189 CO_2 -Pro ATM sensor was deployed, allowing high-frequency (every 4 hours) continuous measurements of
 190 $p\text{CO}_{2\text{sw}}$ and atmospheric $p\text{CO}_2$ ($p\text{CO}_{2\text{atm}}$, μatm) in alternating mode. Pro-Oceanus CO_2 sensors measure dissolved
 191 CO_2 with a semi-permeable membrane, allowing CO_2 in the gas phase to equilibrate with the surrounding water.
 192 The ‘wet’ CO_2 concentration ($x\text{CO}_2$, ppmv) is then detected by an infrared sensor, and the $p\text{CO}_{2\text{sw}}$ (in μatm) is
 193 calculated by multiplying this concentration by the total pressure, in millibars (mbar), within the instrument’s gas
 194 stream:

$$195 \quad p\text{CO}_{2\text{sw}} = x\text{CO}_2 \times \frac{P}{1013.25} \quad (1)$$

197
 198 Long-term signal stability of the data is achieved by an automatic zero compensation function that removes CO_2
 199 from the system at regular intervals and records a new CO_2 baseline value. Both sensors (CO_2 -Pro and CO_2 -Pro
 200 ATM) have a manufacturer stated accuracy of $\pm 5 \mu\text{atm}$. As the first step in the data quality control procedure, the
 201 auto-calibration values following the automatic zero adjustment were discarded. If no stability of the
 202 measurements was detected, also the second and, in some cases, the third values after the automatic zero were
 203 removed. In addition, outliers resulting from sensor malfunctions or maintenance operations were removed.
 204 Calibration by vendors and pre and post deployment checks of the sensors were regularly performed at the in-
 205 house laboratory at OGS, the Calibration and Metrology Center (CTMO), to ensure the quality of the
 206 measurements presented here. Additionally, reference water samples of pH and total alkalinity were collected near
 207 the sensor for the calculation of $p\text{CO}_{2\text{sw}}$. These samples were collected during the annual visits to the EMSO-
 208 E2M3A observatory. Calculations were performed using the CO2SYS software (Pierrot et al., 2006) with the
 209 carbonic acid equilibrium constants (K_1 and K_2) from Lueker et al. (2000), the dissociation constant for HSO_4
 210 from Dickson et al. (1990) and the borate dissociation constant from Lee et al. (2010). The $p\text{CO}_{2\text{sw}}$ from discrete
 211 samples ($p\text{CO}_{2\text{sw}@sample}$, μatm) was matched with the closest hourly $p\text{CO}_{2\text{sw}}$ from sensor ($p\text{CO}_{2\text{sw}@probe}$, μatm)
 212 resulting in the comparison of seven data points in the period 2015 - 2024 (Table 1). When matching within this
 213 short time interval was not possible, a comparison between the $p\text{CO}_{2\text{sw}@sample}$ and the $p\text{CO}_{2\text{sw}@probe}$ with a

214 difference of a few days (no more than one week) was performed. To ensure comparability, $pCO_{2sw@probe}$ was
 215 adjusted to the temperature measured at the time of seawater sampling, which was also used for the determination
 216 of $pCO_{2sw@probe}$, according to Takahashi et al., (1993):

$$217$$

$$218 \quad pCO_{2sw@Tadj} = pCO_{2sw@probe} \times \exp^{(0.0423 \times (T_{probe} - T_{sample}))}$$

219 (2)

220

221 where $pCO_{2sw@Tadj}$ (μatm) is the pCO_{2sw} probe value adjusted for the temperature difference, $pCO_{2sw@probe}$ is
 222 the pCO_{2sw} measured by the probe (μatm), T_{probe} is the temperature ($^{\circ}\text{C}$) measured by the SeaBird SBE 37-ODO
 223 during the acquisition of the $pCO_{2sw@probe}$ and T_{sample} is the temperature ($^{\circ}\text{C}$) measured by the CTD casts during
 224 the collection of the discrete samples.

225

226 **Table 1.** Comparison between pCO_{2sw} from discrete samples ($pCO_{2sw@sample}$, μatm) and pCO_{2sw} from probe ($pCO_{2sw@probe}$,
 227 μatm). The difference is calculated as $pCO_{2sw@sample} - pCO_{2sw@probe}$.

228

Date	$pCO_{2sw@samples}$ (μatm)	$pCO_{2sw@probe}$ (μatm)	Difference (μatm)
20/10/2014	328.11	361.23	-33.12
29/10/2015	381.46	382.63	-1.17
29/07/2017	486.74	480.40	6.34
08/10/2018	381.26	397.50	-16.34
19/10/2019	399.33	379.15	20.18
30/10/2022	383.45	420.90	-37.45
05/12/2023	361.00	364.64	-3.64

229

230 In three out of seven cases, the accuracy of the measurements falls within either the manufacturer's stated accuracy
 231 ($\pm 5 \mu\text{atm}$) or the target accuracy defined by the ICOS network for Fixed Ocean Stations ($\pm 10 \mu\text{atm}$,
 232 <https://www.icos-otc.org/>). In all other cases, these criteria were not met. However, during the recent ICOS Ocean
 233 Thematic Centre (OTC) pCO_2 inter-comparison experiment (Steinhoff et al., 2025), it was demonstrated that
 234 deviations of around 15 - 20 μatm can be expected by membrane sensors, particularly under conditions of
 235 increasing temperature. Additionally, in the two cases of very high deviation, biofouling-likely developing during
 236 the spring/summer period could be identified as a probable contributing factor for this difference. Indeed
 237 continuous monitoring and maintenance of open ocean fixed observatories is often constrained by available
 238 infrastructure, and strict ship time windows influenced by several factors such as weather conditions (Coppola et
 239 al., 2016). Additionally, in 2020, pCO_{2sw} measurements were acquired by two Unmanned Surface Vehicles
 240 (USVs) from Saildrone Inc. (USA) during the ATL2MED demonstration experiment around the EMSO-E2M3A
 241 observatory (Martellucci et al., 2024a; 2025). One of the saildrone was equipped with an ASVCO2 system
 242 developed by PMEL (NOAA's Pacific Marine Environmental Laboratory). This system fed seawater in a bubble

243 equilibrator (Friederich et al., 1995), and the partially dried $x\text{CO}_2$ is measured with an infrared detector (LI-COR
244 820 CO_2 gas analyser). A two-point calibration was used, where the first is a reference gas from NOAA/ESRL,
245 while the second is air purged for CO_2 . Detailed description of the correction, adjustment and quality of $p\text{CO}_{2\text{sw}}$
246 Saildrone data can be found in Martellucci et al. (2024a). A similar trend (significant correlation coefficient of
247 0.77, p -value < 0.01) and a constant offset of 16 μatm between the Saildrone and EMSO-E2M3A data were
248 reported, providing an additional line of evidence for the reliability of this dataset.
249 Due to the limited number of reference water samples and their incomplete representation of the full CO_2 annual
250 cycle, no corrections to the $p\text{CO}_{2\text{sw}}$ data were applied.

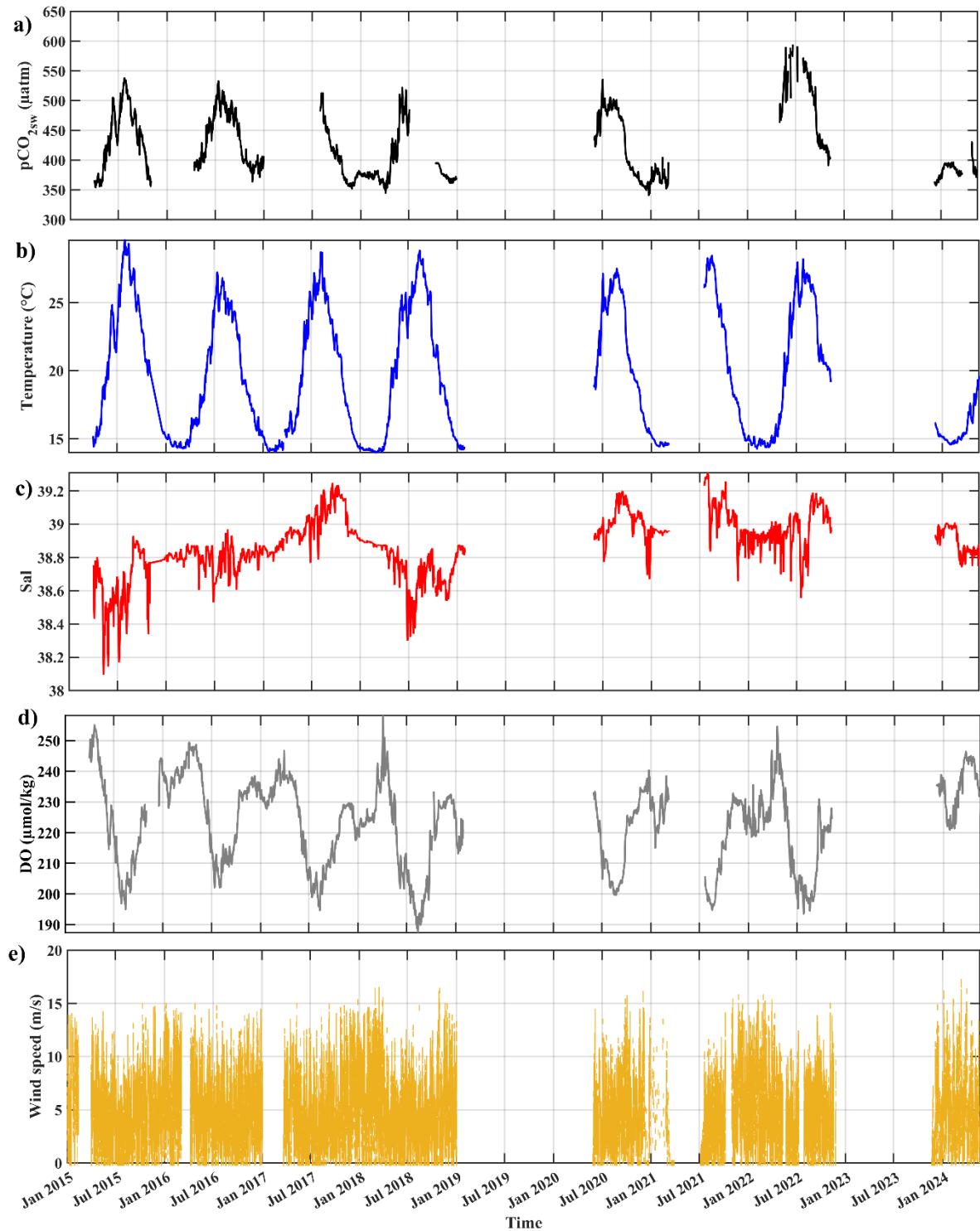
251 **2.2.4. pH data**

252 Hourly pH data were obtained from a SAMI-pH sensor deployed at a depth of 2 meters, covering a two-year
253 period from 2015 to 2016. The instrument uses a high-accuracy colorimetric method, in which seawater is pumped
254 through the sensor and mixed with a pH-sensitive indicator solution (meta-Cresol Purple). According to certified
255 reference material (CRM) intercomparisons, the sensor provides an accuracy of ± 0.003 pH units and a precision
256 of about 0.001 pH units. Calibration by vendors and pre deployment checks of the sensor were performed by the
257 OGS CTMO facility. Discrete samples in the region were also collected in 2015, but no cruises were conducted
258 in the region in 2016. Water samples for validation were collected in 250 mL borosilicate bottles and preserved
259 with mercury chloride (HgCl_2) to prevent biological activity. Samples were stored in the dark and kept cool until
260 laboratory analysis at the OGS facilities. Total scale pH (pH_T) was determined spectrophotometrically following
261 the standard operating procedure SOP 6b described in Dickson et al. (2007). Analyses were performed using a
262 Cary 100 Scan UV-Visible spectrophotometer with a 10 cm pathlength cylindrical quartz cell and a purified 4
263 mM m-Cresol Purple indicator dye. Prior to measurement, samples were equilibrated to 25°C , then subsampled
264 by siphoning through a Tygon tube to avoid gas exchange, ensuring no headspace was present in the cuvette. pH_T
265 was measured immediately after sub-sampling. The precision of the measurements was evaluated on three to five
266 replicates collected from the same Niskin bottle, and was, on average, 0.01%. During the analysis, the temperature
267 of the samples was controlled using a thermostatic cell holders inside the spectrophotometer, connected to a
268 circulation cryothermostat (LAUDA RE415) and monitored with a digital thermometer (VWR Traceable). The
269 mean difference between the three discrete samples and the probe measurements was equal to -0.05 pH units. No
270 further correction to the time series was applied.

271 **3. Robustness and seasonal consistency of the dataset**

272 The surface dataset presented here has been carefully corrected (physical data) and validated (meteorological,
273 $p\text{CO}_2$ and pH data), as described in the previous sections, and all data are publicly available
274 (<https://doi.org/10.13120/y2hw-1j63>, Cardin et al., 2025b). Data gaps were due to maintenance operations,
275 malfunctioning of the sensors and/or the removal of measurements that failed the quality-control procedures
276 described in previous sections. The resulting $p\text{CO}_{2\text{sw}}$ time series (Figure 2a) falls within the expected range of
277 variability for the region. Both the values and seasonal amplitudes are consistent with previous observations in
278 different regions of the Mediterranean Sea (e.g., Pecci et al., 2024; Garcia-Ibañez et al., 2024; Frangoulis et al.,
279 2024; Coppola et al., 2020; Merlivat et al., 2018) and in the Adriatic Sea (e.g., Turk et al., 2010; Cantoni et al.,

280 2012; Ingrosso et al., 2016; Urbini et al., 2020; Cantoni et al., 2024). Lower values are observed in winter, with
281 $p\text{CO}_{2\text{sw}}$ concentrations ranging between 350 and 400 μatm , mainly due to the cooling of the sea surface layer.
282 However, during periods of winter convection and enhanced vertical mixing, $p\text{CO}_{2\text{sw}}$ increases, as observed
283 between December and February in the 2017–2018, 2020–2021, and 2023–2024 periods. In contrast, summer
284 values were around 500 μatm , and in 2022 rise above 550 μatm , closely following surface warming and
285 stratification. Alongside $p\text{CO}_{2\text{sw}}$, other physical and biogeochemical parameters measured at the site further
286 describe the surface layer dynamics. Temperature reflects the seasonal alternation between winter mixing and
287 summer stratification, with values ranging, on average, from 14.87 °C in winter to 25.39 °C in summer (Figure
288 2b). Particularly high temperatures were recorded in 2015, when summer maxima reached 29.6 °C in July. In the
289 following years, summer temperatures remained close to the seasonal average. Interestingly, winter minima
290 showed a gradual increase over time, from values near the seasonal average in the period 2016 - 2019 to an average
291 of around 15.04 °C starting from 2021. Overall, surface temperatures appear slightly higher than those reported
292 for the northwestern Mediterranean (Garcia-Ibañez et al., 2024), especially during the summer months. Marked
293 interannual variability characterizes salinity (Figure 2c), with maximum values exceeding 39 in several years (for
294 instance in 2017, 2020, 2021 and 2022) consistent with previously reported values in the SAP (e.g., Mihanović et
295 al., 2021; Menna et al., 2022). These salinity values are typically higher than those observed in the central
296 Mediterranean (e.g., Lampedusa site, Pecci et al., 2024) or the northwestern Mediterranean (Garcia-Ibañez et al.,
297 2024) reflecting the influence of warm, saline waters of Levantine/Cretan origin entering the area (see Sect. 2.1).
298 Oxygen concentrations follow the expected seasonal dynamics (Figure 2d): lower values are shown during winter
299 mixing, when ventilation dominates, followed by an increase (first peak in the time series) that corresponds to the
300 post-convection bloom. In summer, oxygen concentration decreases again due to respiration processes (e.g.,
301 Martellucci et al., 2024b). Finally, DO increases again at the end of summer (second peak in the time series) due
302 to a smaller bloom occurring in the region during late summer/autumn. Wind speed data (Figure 2e) are also
303 consistent with the regional mean values (e.g., Turk et al., 2010; Pecci et al., 2024) and underline the role of
304 atmospheric forcing in sustaining vertical exchanges, particularly in winter. Mean wind speed value was 5.12 m/s
305 but being frequently higher than 10 m/s. Nevertheless, here an assessment of the main wind regimes in the southern
306 Adriatic was not performed as it was beyond the scope of this manuscript.
307



308

309 **Figure 2.** Time series of sea surface a) partial pressure of CO₂ ($p\text{CO}_{2\text{sw}}$ in μatm); b) Temperature ($^{\circ}\text{C}$); c) Salinity (Sal); d)
 310 dissolved oxygen (DO in $\mu\text{mol}/\text{kg}$); and e) Wind speed (m/s). The variables were measured in the period 2015 - 2024 at EMSO-
 311 E2M3A observatory. Periods of missing data were due to maintenance operations, malfunctioning of the sensors and/or the
 312 removal of measurements that failed the quality-control procedures described in Sect. 2.2..

313

314 A summary of the main biogeochemical and hydrographic variability reported in other Mediterranean regions
 315 from fixed ocean stations in recent years is provided in Table 2.

316

Table 2. Summary of $p\text{CO}_{2\text{sw}}$ and hydrographic variability in other oceanographic regions of the Mediterranean sea.

Observational site	Time span	$p\text{CO}_{2\text{sw}}$	Hydrography	Dissolved oxygen	Wind speed	References
Lampedusa Oceanographic Observatory (Central Mediterranean sea)	December 2021 - June 2023	Seasonal variability: 350 μatm (winter) and 525 μatm (summer)	Salinity ranges: 36.9 - 38.2 Sea surface temperature ranges: 16°C (winter) and 29°C (summer)	-	Wind speed ranges: between 0 m/s and 15 m/s	Pecci et al., 2024
L'Estartit Oceanographic Station and the Blanes Bay Microbial Observatory (Northwestern Mediterranean Sea)	January 2010 - August 2019	Seasonal variability ($f\text{CO}_2$): 350 μatm (winter) and 500 μatm (summer)	Salinity ranges: no clear seasonal cycle, values around 37.9 ± 0.3 Sea surface temperature ranges: 13°C (winter) and 23°C (summer)	-	-	Garcia-Ibañez et al., 2024
BOUSSOLE and DYFAMED sites (Ligurian Sea)	1995–1997 and February 2013 - February 2015	Seasonal variability ($f\text{CO}_2$): 350 μatm (winter) and > 550 μatm (summer) in the 2013 - 2015 period	Mean salinity: values around 38.21 ± 0.03 (1995 - 1997) and 38.19 ± 0.02 (2013 - 2015) Sea surface temperature ranges: 13°C (winter) and 27°C (summer)	-	-	Coppola et al., 2020; Merlivat et al., 2018
POSEIDON fixed platform (Eastern Mediterranean Sea)	January 2020 - May 2023	Seasonal variability: 350 μatm (winter) and ~500 μatm (summer)	Salinity ranges: 39 - 39.6 Sea surface temperature ranges: 15.3°C (winter) and 28.3°C (summer)	-	-	Frangoulis et al., 2024
Gulf of Trieste (Northern Adriatic Sea)	2007-2008; 2008 - 2009; 2011-2013; 2014-2017	Seasonal variability: 220 μatm (winter) and between 475 μatm and 500 μatm (summer)	Salinity ranges: 36 - 37.5 but strong influence of rivers (values < 36) Sea surface temperature ranges: 8°C (winter) and between 26 and 29.5°C (summer)	Dissolved oxygen range: 270 $\mu\text{mol/kg}$ (winter) and around 200 $\mu\text{mol/kg}$ (summer)	Wind speed ranges: between 0 m/s and 15 m/s	Turk et al., 2010; Cantoni et al., 2012; Ingrosso et al., 2016; Urbini et al., 2020; Cantoni et al., 2024

319 Overall, the consistency of seasonal and interannual patterns, and their alignment with well-known physical and
320 biogeochemical drivers such as convection, stratification, and biological activity, strongly support the reliability
321 of the dataset. These results reinforce the robustness of the observations and provide a solid basis for further
322 scientific interpretation.

323 **4. Extended and potential future applications of the dataset: calculation of atmospheric carbon flux (FCO₂)**

324 The dataset presented here can be used to describe physical and biogeochemical properties of surface water in the
325 SAP, as well as to estimate the atmospheric carbon flux (FCO₂). This is essential for evaluating the role of the
326 SAP as a potential carbon source or sink across various temporal scales. Ensuring the reliability of air–sea CO₂
327 flux calculations requires careful evaluation of atmospheric *p*CO₂ and wind speed data, as different
328 parameterizations may need to be applied and some input data recalculated to meet the requirements of the FCO₂
329 formulation. In particular, different parameterizations of the gas transfer velocity could yield divergent results.
330 Equally important is the quality of *p*CO_{2sw} data from sensors. As reported in Steinhoff et al. (2025), it is essential
331 to have a certain degree of knowledge and expertise to produce and interpret optimal quality data, especially for
332 membrane-based systems (such as the submersible Pro-Oceanus sensors) that are easier to operate in the field but
333 require critical understanding of the instrument’s characteristics for data processing. Careful validation and quality
334 control of these input parameters are therefore essential. Addressing these methodological considerations is a
335 prerequisite for producing credible flux estimates and, ultimately, for advancing the understanding of carbon
336 dynamics in the SAP.

337 **5. Data availability**

338 Data described in this work are freely available at the National Oceanographic Data Center (NODC) of the
339 National Institute of Oceanography and Applied Geophysics (<https://doi.org/10.13120/y2hw-1j63>, Cardin et al.,
340 2025b).
341

342 **6. Conclusions**

343 High frequency observations from fixed stations, such as surface buoys and/or moorings, play a crucial role in
344 assessing the regional variability of the carbon cycle in the Mediterranean Sea across different time scales. The
345 dataset presented here provides a comprehensive resource for exploring the biogeochemical and physical
346 dynamics of the sea surface in the dense water formation area of the southern Adriatic Sea. For the first time,
347 high-frequency observations of meteorological, hydrographic and seawater *p*CO₂ and pH data are presented. In
348 addition, the methods used to perform quality control (QC) of the data and possible improvements are discussed.
349 QC is particularly important for *p*CO_{2sw} data as many challenges (such as strict ship time windows) were faced in
350 the region as discussed in Sect. 2.2. Making this time series available for the first time is a significant advancement,
351 particularly considering the strategic importance of the region as a key dense water formation area and for air-sea
352 interaction which are fundamental mechanisms for the capture and storage of atmospheric CO₂. Thus, this dataset
353 provides a valuable example for estimating local surface hydrological and biogeochemical dynamics based on
354 high-resolution regional observations with a high degree of accuracy. This dataset could be also used to
355 characterize carbon flux at the surface in the SAP using only in situ observations, explicitly estimating

356 uncertainties associated with the input variables for CO₂ flux calculations (Sect. 4). In particular, uncertainty
357 related to key parameters such as atmospheric pCO₂ and wind speed, which are typically derived from other
358 observatories or retrieved from models (Ulses et al., 2023). However, some of the data (pCO_{2atm}) currently cover
359 only limited time periods, making data integration necessary to ensure consistency in flux estimates.

360

361 **Author contribution.**

362 CD: data curation, investigation, validation, writing (original draft), writing (review and editing),
363 conceptualisation, formal analysis, software. AR: investigation, writing (review and editing), conceptualisation.
364 GCi: data curation, investigation, validation, writing (review and editing), conceptualisation. MG: data curation,
365 investigation, validation, writing (review and editing), conceptualisation. GCo: investigation, writing (review and
366 editing), conceptualisation. GS: data curation, writing (review and editing), validation, software. SK: data
367 curation, writing (review and editing), validation, software. JLM: data curation, validation, writing (review and
368 editing), software. VC: funding acquisition, project administration, data curation, investigation, validation, writing
369 (review and editing), conceptualisation, supervision.

370

371 **Competing interests.** The contact author has declared that none of the authors has any competing interests.

372

373 **Acknowledgement.**

374 This work benefited from access to E2M3A South Adriatic Regional facility, an EMSO-IT/ICOS-IT and EMSO-
375 ERIC and ICOS Site, operated by OGS. Dataset and activities were partially funded by EMSO Italian Joint
376 Research Unit, by OGS and by the EU - Next Generation EU Mission 4, Component 2, Investment 3.1, "Fund for
377 the realisation of an integrated system of research and innovation infrastructures," for Project IR0000032 –
378 ITINERIS - Italian Integrated Environmental Research Infrastructures System. The authors express their gratitude
379 to the PHYS, BIO and TEC teams, as well as the CTMO units of OGS and to the CNR-ISP, for their essential
380 contributions and continuous efforts in operating and maintaining the EMSO/ICOS-E2M3A regional facility. The
381 authors thank Christian Puntini for his valuable contribution to curating the meteorological data. The author also
382 acknowledges the creators of ChatGPT, used to improve the English writing in some parts of this manuscript.

383

384 **References**

385 Alvarez, M., Catala, S.T., Civitarese, G., Coppola, L., Hassoun, A., Ibello, V., Lazzari, P., Lefevre, D., Macias,
386 D., Santinelli, C., and Ulse, C.: Mediterranean Sea general biogeochemistry, In: Oceanography of the
387 Mediterranean Sea, edited by: Schroeder, K., and Chiggiato, J0., Elsevier, Amsterdam, pp. 387 –451,
388 <https://doi.org/10.1016/B978-0-12-823692-5.00004-2>, 2023.

389 Amorim, F. L. L., Le Meur, J., Wirth, A., and Cardin, V.: Tipping of the double-diffusive regime in the southern
390 Adriatic Pit in 2017 in connection with record high-salinity values, *Ocean Sci.*, 20, 463–474,
391 <https://doi.org/10.5194/os-20-463-2024>, 2024.

392 Artegiani, A., Paschini, E., Russo, A., Bregant, D., Raicich, F., and Pinardi, N.: The Adriatic Sea General
393 Circulation. Part I: Air–Sea Interactions and Water Mass Structure, *J. Phys. Oceanogr.*, 27, 1492–1514,
394 [https://doi.org/10.1175/1520-0485\(1997\)027<1492:tasgcp>2.0.co;2](https://doi.org/10.1175/1520-0485(1997)027<1492:tasgcp>2.0.co;2), 1997.

395 Bensi, M.: Thermohaline variability and mesoscale dynamics observed at the E2M3A deep-site in the south
396 Adriatic sea, PhD thesis, Università degli studi di Trieste, Italy, 2012.

397 Bensi, M., Cardin, V., Rubino, A., Notarstefano, G., and Poulain, P. M.: Effects of winter convection on the deep
398 layer of the Southern Adriatic Sea in 2012: Effects of strong shelf convection, *J. Geophys. Res. Oceans*, 118,
399 6064–6075, <https://doi.org/10.1002/2013jc009432>, 2013.

400 Bensi, M., Cardin, V., and Rubino, A.: Thermohaline variability and mesoscale dynamics observed at the deep-
401 ocean observatory E2M3A in the southern Adriatic sea, in *The Mediterranean Sea: Temporal Variability and*
402 *Spatial Patterns*, Geophysical Monograph Series, eds G. L. E. Borzelli, M. Gačić, P. Lionello, and P. Malanotte-
403 Rizzoli (Oxford, UK: John Wiley & Sons, Inc.), 139–155, <https://doi.org/10.1002/9781118847572.ch9>, 2014.

404 Bignami, F., Salusti, E., and Schiarini, S.: Observations on a bottom vein of dense water in the southern Adriatic
405 and Ionian seas, *J. Geophys. Res.*, 95, 7249–7259, <https://doi.org/10.1029/jc095ic05p07249>, 1990.

406 Bozzano, R., Pensieri, S., Pensieri, L., Cardin, V., Brunetti, F., Bensi, M., Petihakis, G., Tsagaraki, T. M.,
407 Ntoumas, M., Podaras, D., and Perivoliotis, L.: The M3A network of open ocean observatories in the
408 Mediterranean Sea, in: 2013 MTS/IEEE OCEANS-Bergen, IEEE, Bergen, Norway, 10–14 June 2013, 1–10,
409 <https://doi.org/10.1109/OCEANS-Bergen.2013.6607996>, 2013.

410 Bunsen, F., Nissen, C., and Hauck, J.: The Impact of Recent Climate Change on the Global Ocean Carbon Sink,
411 *Geophysical Research Letters*, 51, <https://doi.org/10.1029/2023gl1107030>, 2024.

412 Cantoni, C., Luchetta, A., Celio, M., Cozzi, S., Raichich, F., and Catalano, G.: Carbonate system variability in the
413 Gulf of Trieste (North Adriatic Sea), *Estuarine, Coastal and Shelf Science*, 115, 51–62,
414 <https://doi.org/10.1016/j.ecss.2012.07.006>, 2012.

415 Cantoni, C., Luchetta, A., Chiggiato, J., Cozzi, S., Schroeder, K., and Langone, L.: Dense water flow and
416 carbonate system in the southern Adriatic: A focus on the 2012 event, *Marine Geology*, 375, 15–27,
417 <https://doi.org/10.1016/j.margeo.2015.08.013>, 2016.

418 Cantoni, C., De Vittor, C., Faganeli, J., Giani, M., Kovač, N., Malej, A., Ogrinc, N., Tamše, S., and Turk, V.:
419 Carbonate system and acidification of the Adriatic Sea, *Marine Chemistry*, 267, 104462,
420 <https://doi.org/10.1016/j.marchem.2024.104462>, 2024.

421 Cardin, V., Bensi, M., and Pacciaroni, M.: Variability of water mass properties in the last two decades in the South
422 Adriatic Sea with emphasis on the period 2006–2009, *Continental Shelf Research*, 31, 951–965,
423 <https://doi.org/10.1016/j.csr.2011.03.002>, 2011.

424 Cardin V., Siena, G., Giorgetti, A., Ursella, L., Brosich, A., and Partescano, E.: The Ritmare Fixed Sites Network
425 Procedures for Real-Time Data Quality Control, <https://doi.org/10.13140/RG.2.2.31100.44166>, 2014.

426 Cardin, V., Wirth, A., Khosravi, M., and Gačić, M.: South Adriatic Recipes: Estimating the Vertical Mixing in
427 the Deep Pit, *Front. Mar. Sci.*, 7, <https://doi.org/10.3389/fmars.2020.565982>, 2020.

- 428 Cardin, V., Le Meur, J., Ursella, L., Dentico, C., Siena, G., Mansutti, P., Brunetti, F., and Partescano, E.: EMSO-
429 E2M3A-Water-Column-time-series-South-Adriatic [dataset], <https://doi.org/10.13120/ZE9Q-3E51>, 2025a.
- 430 Cardin, V., Dentico, C., Brunetti, F., Bubbi, A., Chiaruttini, L., Civitarese, G., Comici, C., Corbo, A., Gerin, R.,
431 Giani, M., Kuchler, S., Le Meur, J., Mansutti, P., Savonitto, G. and Siena, G.: EMSO-E2M3A-B-Surface-time-
432 series-South-Adriatic [dataset], <https://doi.org/10.13120/y2hw-1j63>, 2025b.
- 433 Civitarese, G., Gačić, M., Batistić, M., Bensi, M., Cardin, V., Dulčić, J., Garić, R., and Menna, M.: The BiOS
434 mechanism: History, theory, implications, *Progress in Oceanography*, 216, 103056,
435 <https://doi.org/10.1016/j.pocean.2023.103056>, 2023.
- 436 Coppola, L., Ntoumas, M., Bozzano, R., Bensi, M., Hartman, S. E., Charcos Llorens, M., Craig, J., Rolin, J-F.,
437 Giovanetti, G., Cano, D., Karstensen, J., Cianca, A., Toma, D., Stasch, C., Pensieri, S., Cardin, V., Tengberg, A.,
438 Petihakis, G., and Cristini, L.: Handbook of Best Practices for Open Ocean Fixed Observatories, FixO3 Project,
439 127, FP7 Programme 2007–2013 under grant agreement no 312463, European Commission, 2016.
- 440 CO₂.Earth: <http://co2.earth/>, last access: 14 July 2025.
- 441 Dickson, A.G.: Thermodynamics of the dissociation of boric acid and synthetic seawater from 273.15 to 318.15 K.
442 *Deep -Sea Res.* 137, 755 –766, 1990.
- 443 Dickson, A., Sabine, C., and Christian, J.R.: Guide to best practice for ocean CO₂ measurements. *PICES Special*
444 *Publ.* 3, 2007.
- 445 Fedele, G., Mauri, E., Notarstefano, G., and Poulain, P. M.: Characterization of the Atlantic Water and Levantine
446 Intermediate Water in the Mediterranean Sea using Argo Float Data. *Ocean Science Discussions*, 1-41,
447 <https://doi.org/10.5194/os-18-129-2022>, 2021.
- 448 Frangoulis, C., Stamataki, N., Pettas, M., Michelinakis, S., King, A. L., Giannoudi, L., Tsiaras, K., Christodoulaki,
449 S., Seppälä, J., Thyssen, M., Borges, A. V., and Krasakopoulou, E.: A carbonate system time series in the Eastern
450 Mediterranean Sea. Two years of high-frequency in-situ observations and remote sensing, *Front. Mar. Sci.*, 11,
451 1348161, <https://doi.org/10.3389/fmars.2024.1348161>, 2024.
- 452 Friederich, G. E., Brewer, P. G., Herlien, R., and Chavez, F. P.: Measurement of sea surface partial pressure of
453 CO₂ from a moored buoy, *Deep-Sea Res. Pt. I*, 42, 1175–1186, [https://doi.org/10.1016/0967-0637\(95\)00044-7](https://doi.org/10.1016/0967-0637(95)00044-7),
454 1995.
- 455 Friedlingstein, P., O’Sullivan, M., Jones, M. W., Andrew, R. M., Hauck, J., Landschützer, P., Le Quéré, C., Li,
456 H., Luijkx, I. T., Olsen, A., Peters, G. P., Peters, W., Pongratz, J., Schwingshackl, C., Sitch, S., Canadell, J. G.,
457 Ciais, P., Jackson, R. B., Alin, S. R., Arneeth, A., Arora, V., Bates, N. R., Becker, M., Bellouin, N., Berghoff, C.
458 F., Bittig, H. C., Bopp, L., Cadule, P., Campbell, K., Chamberlain, M. A., Chandra, N., Chevallier, F., Chini, L.
459 P., Colligan, T., Decayeux, J., Djeutchouang, L., Dou, X., Duran Rojas, C., Enyo, K., Evans, W., Fay, A., Feely,
460 R. A., Ford, D. J., Foster, A., Gasser, T., Gehlen, M., Gkritzalis, T., Grassi, G., Gregor, L., Gruber, N., Gürses,
461 Ö., Harris, I., Hefner, M., Heinke, J., Hurtt, G. C., Iida, Y., Ilyina, T., Jacobson, A. R., Jain, A., Jarníková, T.,
462 Jersild, A., Jiang, F., Jin, Z., Kato, E., Keeling, R. F., Klein Goldewijk, K., Knauer, J., Korsbakken, J. I., Lauvset,

463 S. K., Lefèvre, N., Liu, Z., Liu, J., Ma, L., Maksyutov, S., Marland, G., Mayot, N., McGuire, P., Metzl, N.,
464 Monacci, N. M., Morgan, E. J., Nakaoka, S.-I., Neill, C., Niwa, Y., Nützel, T., Olivier, L., Ono, T., Palmer, P. I.,
465 Pierrot, D., Qin, Z., Resplandy, L., Roobaert, A., Rosan, T. M., Rödenbeck, C., Schwinger, J., Smallman, T. L.,
466 Smith, S., Sospedra-Alfonso, R., Steinhoff, T., Sun, Q., et al.: Global Carbon Budget 2024,
467 <https://doi.org/10.5194/essd-2024-519>, 13 November 2024.

468 Gačić, M., Marullo, S., Santoleri, R., and Bergamasco, A.: Analysis of the seasonal and interannual variability of
469 the sea surface temperature field in the Adriatic Sea from AVHRR data (1984–1992), *J. Geophys. Res.*, 102,
470 22937–22946, <https://doi.org/10.1029/97jc01720>, 1997.

471 Gačić, M., Civitarese, G., Eusebi Borzelli, G. L., Kovačević, V., Poulain, P.-M., Theocharis, A., Menna, M.,
472 Catucci, A., and Zarokanellos, N.: On the relationship between the decadal oscillations of the northern Ionian Sea
473 and the salinity distributions in the eastern Mediterranean, *J. Geophys. Res.*, 116,
474 <https://doi.org/10.1029/2011jc007280>, 2011.

475 García-Ibáñez, M. I., Gualart, E. F., Lucas, A., Pascual, J., Gasol, J. M., Marrasé, C., Calvo, E., and Pelejero, C.:
476 Two new coastal time-series of seawater carbonate system variables in the NW Mediterranean Sea: rates and
477 mechanisms controlling pH changes, *Front. Mar. Sci.*, 11, <https://doi.org/10.3389/fmars.2024.1348133>, 2024.

478 Gattuso, J-P, and Hansson L. (Eds). *Ocean acidification*. Oxford university press, 2011.

479 Hassoun, A. E. R., Gemayel, E., Krasakopoulou, E., Goyet, C., Abboud-Abi Saab, M., Guglielmi, V., Touratier,
480 F., and Falco, C.: Acidification of the Mediterranean Sea from anthropogenic carbon penetration, *Deep Sea*
481 *Research Part I: Oceanographic Research Papers*, 102, 1–15, <https://doi.org/10.1016/j.dsr.2015.04.005>, 2015.

482 Hassoun, A. E. R., Bantelman, A., Canu, D., Comeau, S., Galdies, C., Gattuso, J.-P., Giani, M., Grelaud, M.,
483 Hendriks, I. E., Ibello, V., Idrissi, M., Krasakopoulou, E., Shaltout, N., Solidoro, C., Swarzenski, P. W., and
484 Ziveri, P.: Ocean acidification research in the Mediterranean Sea: Status, trends and next steps, *Front. Mar. Sci.*,
485 9, <https://doi.org/10.3389/fmars.2022.892670>, 2022.

486 ICOS-Ocean Thematic Center: <https://www.icos-otc.org/>, last access: 14 October 2025.

487 Intergovernmental Panel on Climate Change (IPCC). *Changing State of the Climate System*. In: *Climate Change*
488 *2021 – The Physical Science Basis: Working Group I Contribution to the Sixth Assessment Report of the*
489 *Intergovernmental Panel on Climate Change*. Cambridge University Press; 2023:287-422, 2021.

490 Ingrosso, G., Giani, M., Comici, C., Kralj, M., Piacentino, S., De Vittor, C., and Del Negro, P.: Drivers of the
491 carbonate system seasonal variations in a Mediterranean gulf, *Estuarine, Coastal and Shelf Science*, 168, 58–70,
492 <https://doi.org/10.1016/j.ecss.2015.11.001>, 2016.

493 Ingrosso, G., Bensi, M., Cardin, V., and Giani, M.: Anthropogenic CO₂ in a dense water formation area of the
494 Mediterranean Sea, *Deep Sea Research Part I: Oceanographic Research Papers*, 123, 118–128,
495 <https://doi.org/10.1016/j.dsr.2017.04.004>, 2017.

496 IOC UNESCO: <https://www.ioc.unesco.org/en>, last access: 21 July 2025.

497 Kapsenberg, L., Alliouane, S., Gazeau, F., Mousseau, L., and Gattuso, J.-P.: Concomitant ocean acidification and
498 increasing total alkalinity at a coastal site in the NW Mediterranean Sea (2007-2015), [https://doi.org/10.5194/os-](https://doi.org/10.5194/os-2016-71)
499 [2016-71](https://doi.org/10.5194/os-2016-71), 13 September 2016.

500 Lazoglou, G., Papadopoulos-Zachos, A., Georgiades, P., Zittis, G., Velikou, K., Manios, E. M., and
501 Anagnostopoulou, C.: Identification of climate change hotspots in the Mediterranean, *Sci Rep*, 14, 29817,
502 <https://doi.org/10.1038/s41598-024-80139-1>, 2024.

503 Lee, K., Kim, T. -W., Byrne, R.H., Millero, F.J., Feely, R.A., Liu, Y -M.: The universal ratio of boron to chlorinity
504 for the North Pacific and North Atlantic oceans. *Geochim. Cosmochim. Acta* 74, 1801 –1811, 2010.

505 Lueker, T. J., Dickson, A. G., and Keeling, C. D.: Ocean pCO₂ calculated from dissolved inorganic carbon,
506 alkalinity, and equations for K₁ and K₂: Validation based on laboratory measurements of CO₂ in gas and seawater
507 at equilibrium. *Mar. Chem.* 70, 105 –119, 2000.

508 Le Meur, J., Wirth, A., Paladini De Mendoza, F., Miserocchi, S., and Cardin, V.: Intermittent supply of dense
509 water to the deep South Adriatic Pit: an observational study, *Front. Mar. Sci.*, 12,
510 <https://doi.org/10.3389/fmars.2025.1516780>, 2025.

511 Malanotte-Rizzoli, P.: The Northern Adriatic Sea as a prototype of convection and water mass formation on the
512 continental shelf P.C Chu, J.C Gascard (Eds.), *Deep Convection and Deep Water Formation in the Oceans*,
513 Elsevier Oceanography Series, vol. 57, Elsevier, Amsterdam, pp. 229-239, 1991.

514 Martellucci, R., Giani, M., Mauri, E., Coppola, L., Paulsen, M., Fourier, M., Pensieri, S., Cardin, V., Dentico,
515 C., Bozzano, R., Cantoni, C., Lucchetta, A., Izquierdo, A., Bruno, M., and Skjelvan, I.: CO₂ and hydrography
516 acquired by autonomous surface vehicles from the Atlantic Ocean to the Mediterranean Sea: data correction and
517 validation, *Earth Syst. Sci. Data*, 16, 5333–5356, <https://doi.org/10.5194/essd-16-5333-2024>, 2024a.

518 Martellucci, R., Menna, M., Mauri, E., Pirro, A., Gerin, R., Paladini De Mendoza, F., Garić, R., Batistić, M., Di
519 Biagio, V., Giordano, P., Langone, L., Miserocchi, S., Gallo, A., Notarstefano, G., Savonitto, G., Bussani, A.,
520 Pacciaroni, M., Zuppelli, P., and Poulain, P.-M.: Recent changes of the dissolved oxygen distribution in the deep
521 convection cell of the southern Adriatic Sea, *Journal of Marine Systems*, 245, 103988,
522 <https://doi.org/10.1016/j.jmarsys.2024.103988>, 2024b.

523 Martellucci, R., Dentico, C., Coppola, L., Skjelvan, I., Giani, M., Pensieri, S., Cantoni, C., Cardin, V., Fourier,
524 M., Bozzano, R., Paulsen, M., and Mauri, E.: Air-sea CO₂ exchange in the Eastern Atlantic and the Mediterranean
525 Sea based on autonomous surface measurements, 2025. In review.

526 Menna, M., Martellucci, R., Notarstefano, G., Mauri, E., Gerin, R., Pacciaroni, M., Bussani, A., Pirro, A., Poulain,
527 P.-M.: Record-breaking high salinity in the South Adriatic Pit in 2020, in: Copernicus Ocean State Report, issue
528 6. *Journal of Operational Oceanography*, 15(sup1), 1–220. <https://doi.org/10.1080/1755876X.2022.2095169>,
529 2022.

530 Merlivat, L., Boutin, J., Antoine, D., Beaumont, L., Golbol, M., and Vellucci, V.: Increase of dissolved inorganic
531 carbon and decrease in pH in near-surface waters in the Mediterranean Sea during the past two decades,
532 *Biogeosciences*, 15, 5653–5662, <https://doi.org/10.5194/bg-15-5653-2018>, 2018.

533 Mihanović, H., Vilibić, I., Šepić, J., Matic, F., Ljubešić, Z., Mauri, E., Gerin, R., Notarstefano, G., and Poulain,
534 P.-M.: Observation, Preconditioning and Recurrence of Exceptionally High Salinities in the Adriatic Sea, *Front.*
535 *Mar. Sci.*, 8, 672210, <https://doi.org/10.3389/fmars.2021.672210>, 2021.

536 Ovchinnikov, I.M., Zats, V.I., Krivosheya, V.G., and Udodov, A.I.: Formation of deep Eastern Mediterranean
537 waters in the Adriatic Sea. *Oceanology*, 25, 6, 704-707, 1985.

538 Orr, J. C., Epitalon, J.-M., and Gattuso, J.-P.: Comparison of ten packages that compute ocean carbonate
539 chemistry, *Biogeosciences*, 12, 1483–1510, <https://doi.org/10.5194/bg-12-1483-2015>, 2015.

540 Oudot, C., Gerard, R., Morin, P.: Precise shipboard determination of dissolved oxygen (Winkler procedure) for
541 productivity studies with commercial system. *Limnology and Oceanography* 33, 146e150, 1988.

542 Pecci, M., Sferlazzo, D., Anello, F., Becagli, S., Colella, S., Silvestri, L. D., Iorio, T. D., Meloni, D., Monteleone,
543 F., Piacentino, S., Principato, E., and Sarra, A. D.: Large influence of the 2022-23 marine heatwave on the air-sea
544 CO₂ flux in the Central Mediterranean, <https://doi.org/10.22541/essoar.173393985.55347710/v1>, 11 December
545 2024.

546 Pierrot, D., Lewis, E., and Wallace, D. W. R.: MS Excel Program Developed for CO₂ system calculations.
547 https://cdiac.ess -drive.lbl.gov/ftp/co2sys/CO2SYS_calc_XLS_v2.1/, 2006.

548 Ravaioli, M., Bergami, C., Riminucci, F., Langone, L., Cardin, V., Di Sarra, A., Aracri, S., Bastianini, M., Bensi,
549 M., Bergamasco, A., Bommarito, C., Borghini, M., Bortoluzzi, G., Bozzano, R., Cantoni, C., Chiggiato, J., Crisafi,
550 E., D'Adamo, R., Durante, S., Fanara, C., Grilli, F., Lipizer, M., Marini, M., Miseroocchi, S., Paschini, E., Penna,
551 P., Pensieri, S., Pugnetti, A., Raicich, F., Schroeder, K., Siena, G., Specchiulli, A., Stanghellini, G., Vetrano, A.,
552 and Crise, A.: The RITMARE Italian Fixed-Point Observatory Network (IFON) for marine environmental
553 monitoring: a case study, *Journal of Operational Oceanography*, 9, s202–s214,
554 <https://doi.org/10.1080/1755876x.2015.1114806>, 2016.

555 Riebesell, U., Gattuso, J. P., Thingstad, T. F., & Middelburg, J. J.: Arctic ocean acidification: pelagic ecosystem
556 and biogeochemical responses during a mesocosm study. *Biogeosciences*, 10, 5619-5626, doi:10.5194/bg-10-
557 5619-2013, 2013.

558 Robinson, A.R., Leslie, W.G., Theocharis, A., and Lascaratos, A.: Mediterranean Sea circulation. *Encyclopedia*
559 *of Ocean Sciences Academic Press, Harcourt Science & Technology, Harcourt Place, 32 Jamestown Road London*
560 *NW1 7BY UK, pp. 1689–1705, 2001.*

561 Roether, W. and Schlitzer, R.: Eastern Mediterranean deep water renewal on the basis of chlorofluoromethane
562 and tritium data, *Dynamics of Atmospheres and Oceans*, 15, 333–354, [https://doi.org/10.1016/0377-
563 0265\(91\)90025-b](https://doi.org/10.1016/0377-0265(91)90025-b), 1991.

564 Schlitzer, R., Roether, W., Oster, H., Junghans, H.-G., Hausmann, M., Johannsen, H., and Michelato, A.:
565 Chlorofluoromethane and oxygen in the Eastern Mediterranean, Deep Sea Research Part A. Oceanographic
566 Research Papers, 38, 1531–1551, [https://doi.org/10.1016/0198-0149\(91\)90088-w](https://doi.org/10.1016/0198-0149(91)90088-w), 1991.

567 Schneider, A., Tanhua, T., Körtzinger, A., and Wallace, D. W. R.: High anthropogenic carbon content in the
568 eastern Mediterranean, J. Geophys. Res., 115, <https://doi.org/10.1029/2010jc006171>, 2010.

569 Schroeder, K., Ben Ismail, S., Bensi, M., Bosse, A., Chiggiato, J., Civitarese, G., Falcieri M, F., Fusco, G., Gačić,
570 M., Gertman, I., Kubin, E., Malanotte-Rizzoli, P., Martellucci, R., Menna, M., Ozer, T., Taupier-Letage, I.,
571 Vargas-Yáñez, M., Velaoras, D., and Vilibić, I.: A consensus-based, revised and comprehensive catalogue for
572 Mediterranean water masses acronyms. Mediterranean Marine Science, 25(3), 783–791.
573 <https://doi.org/10.12681/mms.38736>, 2024.

574 Steinhoff, T., Gkritzalis, T., Jones, S., Macovei, V. A., Neill, C., Schuster, U., Akl, J., Arruda, R., Atamanchuk,
575 D., Barry, M., Beaumont, L., Cantoni, C., Dickson, A., Fahning, J., Fought, J., Frangoulis, C., Gutiérrez-Loza, L.,
576 Hagan, C., Honkanen, M., Kielosto, S., Kinski, N., Körtzinger, A., Landschützer, P., Lauvset, S. K., Lawrence-
577 Slavass, N., Li, Q., Luchetta, A., Malarde, D., Paulsen, M., Ritschel, M., Rutgersson, A., Sanders, R., Shitashima,
578 K., Spaulding, R., Stamatakis, N., Stenbäck, K., Sutton, A., Tatkiewicz, W., Telszewski, M., Theetaert, H.,
579 Tilbrook, B., and Wanninkhof, R.: The ICOS OTC P CO₂ instrument intercomparison, Limnology & Ocean
580 Methods, lom3.10727, <https://doi.org/10.1002/lom3.10727>, 2025.

581 Taillandier, V., D’Ortenzio, F., Prieur, L., Conan, P., Coppola, L., Cornec M., Dumas F., Durrieu de Madron X. ,
582 Fach B., Fourrier M., Gentil M., Hayes D., Husrevoglu S., Legoff H., Le Sterl L., Örek H., Ozer T., Poulain P.
583 M., Pujo-Pay M., Ribera d’Alcalà M., Salihoglu B., Testor P., Velaoras D., Wagener T., and Wimart-Rousseauet
584 C.: Sources of the Levantine intermediate water in winter 2019. Journal of Geophysical Research: Oceans, 127,
585 <https://doi.org/10.1029/2021JC017506>, 2022.

586 Takahashi, T., Olafsson, J., Goddard, J. G., Chipman, D. W., and Sutherland, S. C.: Seasonal variation of CO₂
587 and nutrients in the high-latitude surface oceans: A comparative study, Global Biogeochemical Cycles, 7, 843–
588 878, <https://doi.org/10.1029/93GB02263>, 1993.

589 Takahashi, T., Sutherland, S. C., Wanninkhof, R., Sweeney, C., Feely, R. A., Chipman, D. W., Hales, B.,
590 Friederich, G., Chavez, F., Sabine, C., Watson, A., Bakker, D. C. E., Schuster, U., Metzl, N., Yoshikawa-Inoue,
591 H., Ishii, M., Midorikawa, T., Nojiri, Y., Körtzinger, A., Steinhoff, T., Hoppema, M., Olafsson, J., Arnarson, T.
592 S., Tilbrook, B., Johannessen, T., Olsen, A., Bellerby, R., Wong, C. S., Delille, B., Bates, N. R., and De Baar, H.
593 J. W.: Climatological mean and decadal change in surface ocean pCO₂, and net sea–air CO₂ flux over the global
594 oceans, Deep Sea Research Part II: Topical Studies in Oceanography, 56, 554–577,
595 <https://doi.org/10.1016/j.dsr2.2008.12.009>, 2009.

596 The MathWorks Inc. MATLAB version: 9.13.0 (R2023b), Natick, Massachusetts: The MathWorks Inc.
597 <https://www.mathworks.com>, 2022.

598 Touratier, F. and Goyet, C.: Impact of the Eastern Mediterranean Transient on the distribution of anthropogenic
599 CO₂ and first estimate of acidification for the Mediterranean Sea, *Deep Sea Research Part I: Oceanographic*
600 *Research Papers*, 58, 1–15, <https://doi.org/10.1016/j.dsr.2010.10.002>, 2011.

601 Turk, D., Malačič, V., DeGrandpre, M. D., and McGillis, W. R.: Carbon dioxide variability and air-sea fluxes in
602 the northern Adriatic Sea, *J. Geophys. Res.*, 115, 2009JC006034, <https://doi.org/10.1029/2009JC006034>,
603 2010.

604 Ulses, C., Estournel, C., Marsaleix, P., Soetaert, K., Fourier, M., Coppola, L., Lefèvre, D., Touratier, F., Goyet,
605 C., Guglielmi, V., Kessouri, F., Testor, P., and Durrieu De Madron, X.: Seasonal dynamics and annual budget of
606 dissolved inorganic carbon in the northwestern Mediterranean deep-convection region, *Biogeosciences*, 20, 4683–
607 4710, <https://doi.org/10.5194/bg-20-4683-2023>, 2023.

608 Urbini, L., Ingrosso, G., Djakovac, T., Piacentino, S., and Giani, M.: Temporal and Spatial Variability of the CO₂
609 System in a Riverine Influenced Area of the Mediterranean Sea, the Northern Adriatic, *Front. Mar. Sci.*, 7,
610 <https://doi.org/10.3389/fmars.2020.00679>, 2020.

611 Urdiales-Flores, D., Zittis, G., Hadjinicolaou, P., Osipov, S., Klingmüller, K., Mihalopoulos, N., Kanakidou, M.,
612 Economou, T., and Lelieveld, J.: Drivers of accelerated warming in Mediterranean climate-type regions, *npj Clim*
613 *Atmos Sci*, 6, 97, <https://doi.org/10.1038/s41612-023-00423-1>, 2023.

614 Vilibić, I. and Orlić, M.: Least-squares tracer analysis of water masses in the South Adriatic (1967–1990), *Deep*
615 *Sea Research Part I: Oceanographic Research Papers*, 48, 2297–2330, [https://doi.org/10.1016/s0967-](https://doi.org/10.1016/s0967-0637(01)00014-0)
616 [0637\(01\)00014-0](https://doi.org/10.1016/s0967-0637(01)00014-0), 2001.

617 Zittis, G., Hadjinicolaou, P., Klangidou, M., Proestos, Y., and Lelieveld, J.: A multi-model, multi-scenario, and
618 multi-domain analysis of regional climate projections for the Mediterranean, *Reg Environ Change*, 19, 2621–
619 2635, <https://doi.org/10.1007/s10113-019-01565-w>, 2019.

620